Applied Catalysis B: Environmental 100 (2010) 433–439

Contents lists available at ScienceDirect

Applied Catalysis B: Environmental

journal homepage: www.elsevier.com/locate/apcatb

$NaYF_4$:Yb,Tm/CdS composite as a novel near-infrared-driven photocatalyst

Chuanhao Li[a], Feng Wang[a], Jian Zhu[a,b], Jimmy C. Yu[a,*]

[a] Department of Chemistry, Environmental Science Programme and Centre of Novel Functional Materials, The Chinese University of Hong Kong, Shatin, New Territories, Hong Kong, China
[b] Department of Chemistry, Shanghai Normal University, Shanghai, China

ARTICLE INFO

Article history:
Received 11 May 2010
Received in revised form 16 August 2010
Accepted 20 August 2010
Available online 27 August 2010

Keywords:
Near infrared
Photocatalysis
Upconversion

ABSTRACT

We report on the preparation of a novel near infrared photocatalyst by combining a low energy band gap semiconductor CdS with an upconversion material $NaYF_4$:Yb,Tm. Particles of CdS and $NaYF_4$:Yb,Tm are pretreated with thioglycolic acid and mercaptoethanol. The reaction between these two organic molecules causes the formation of $NaYF_4$:Yb,Tm/CdS composite. Results from scanning electron microscopy (SEM), transmission electron microscopy (TEM), energy-dispersive X-ray spectroscopy (EDX) and powder X-ray diffraction (XRD) measurements demonstrate that CdS nanoparticles are uniformly assembled on the surface of $NaYF_4$:Yb,Tm microrods. Energy transfer from $NaYF_4$:Yb,Tm to CdS is confirmed by the upconversion and fluorescence decay properties. Hydroxyl radicals are generated upon NIR irradiation on the composite material. The NIR photocatalytic activity of the $NaYF_4$:Yb,Tm/CdS composite is investigated by degrading Rhodamine B and methylene blue. A mechanism for NIR-driven photocatalysis is proposed.

1. Introduction

Photocatalysis is an environmentally friendly technique to eliminate toxic organic substances in air and water. The process is initiated by the irradiation of semiconductor materials with a suitable light source. The subsequently formed free radicals with strong oxidizing ability could mineralize organic pollutants to CO_2 and H_2O [1]. Photocatalysis has attracted much attention in recent years because it allows the utilization of clean, safe, and renewable solar energy to solve environmental problems.

Fujishima and Honda discovered the photocatalytic splitting of water on titanium dioxide (TiO_2) photoanodes under ultraviolet (UV) light in 1972 [2]. Since then TiO_2 has been widely studied as an efficient photocatalyst for its appropriate electronic band structure, biological and chemical inertness, strong oxidizing power and long-term stability [3]. However, this photocatalyst has a relatively large band gap that requires UV light for activation. Much effort has been focused on improving the photocatalytic efficiency by understanding the effects of particle size, morphology, crystal structure, surface area on the reaction mechanism [4–8].

Various approaches have been developed to extend the response of photocatalysts into the visible-light region. These include doping metallic (Pt [9], Fe [10], Ag [11], Cr [12]) and nonmetallic (C [13], N [14], F [15], S [16]) elements in conventional photocatalysts to decrease the band gap to accommodate the visible-light photon energy, and the use of some low band gap semiconductors including CdS [17,18], WO_3 [19,20], $BiVO_4$ [21], Bi_2WO_6 [22], and polymeric semiconductors [23]. Another promising system is the coupled semiconductor such as TiO_2/CdS [24,25], in which CdS absorbs visible-light and transfers the photoexcited electrons to TiO_2 to induce photoreactions.

Near infrared (NIR) photocatalysis involving YF_3:Yb,Tm/TiO_2 core/shell nanoparticles has been reported recently [26]. The upconversion YF_3:Yb,Tm particles absorb NIR light and emit a very weak UV light which excites TiO_2 for photocatalysis. NIR to UV conversion is obviously a difficult process, and it would be much easier to convert NIR to visible-light [27–31]. It is widely accepted that the hexagonal phase of $NaYF_4$ is a better host material for upconverting NIR to visible-light than the nonlinear crystals [27–32]. For example, the efficiency for $NaYF_4$:Yb,Tm is 3.4×10^{-2} cm^2/W while that for potassium dihydrogen phosphate (KDP) is only in the order of 10^{-11} [32]. Fig. S1 (see supporting information) shows the large difference in intensity between UV and visible-light emissions from NIR-excited YF_3:Yb,Tm and $NaYF_4$:Yb,Tm. To take advantage of the much stronger visible-light emission, it would be a good idea to replace TiO_2 with a narrower bandgap CdS. Herein, we describe an efficient approach to construct NIR photocatalyst composed of $NaYF_4$:Yb,Tm and CdS. After capturing NIR photons, $NaYF_4$:Yb,Tm emits relatively strong visible-light which matches very well with the band gap of CdS. The composite material is found effective for NIR-induced photocatalytic degradation of dyes.

* Corresponding author. Tel.: +852 26096268; fax: +852 26035057.
E-mail address: jimyu@cuhk.edu.hk (J.C. Yu).

0926-3373/$ – see front matter © 2010 Elsevier B.V. All rights reserved.
doi:10.1016/j.apcatb.2010.08.017

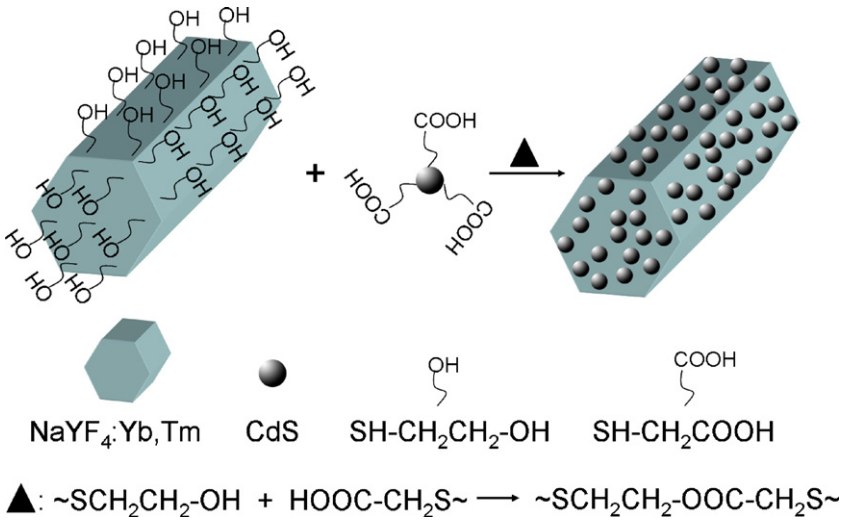

Scheme 1. Strategy for the preparation of $NaYF_4$:Yb,Tm/CdS composite.

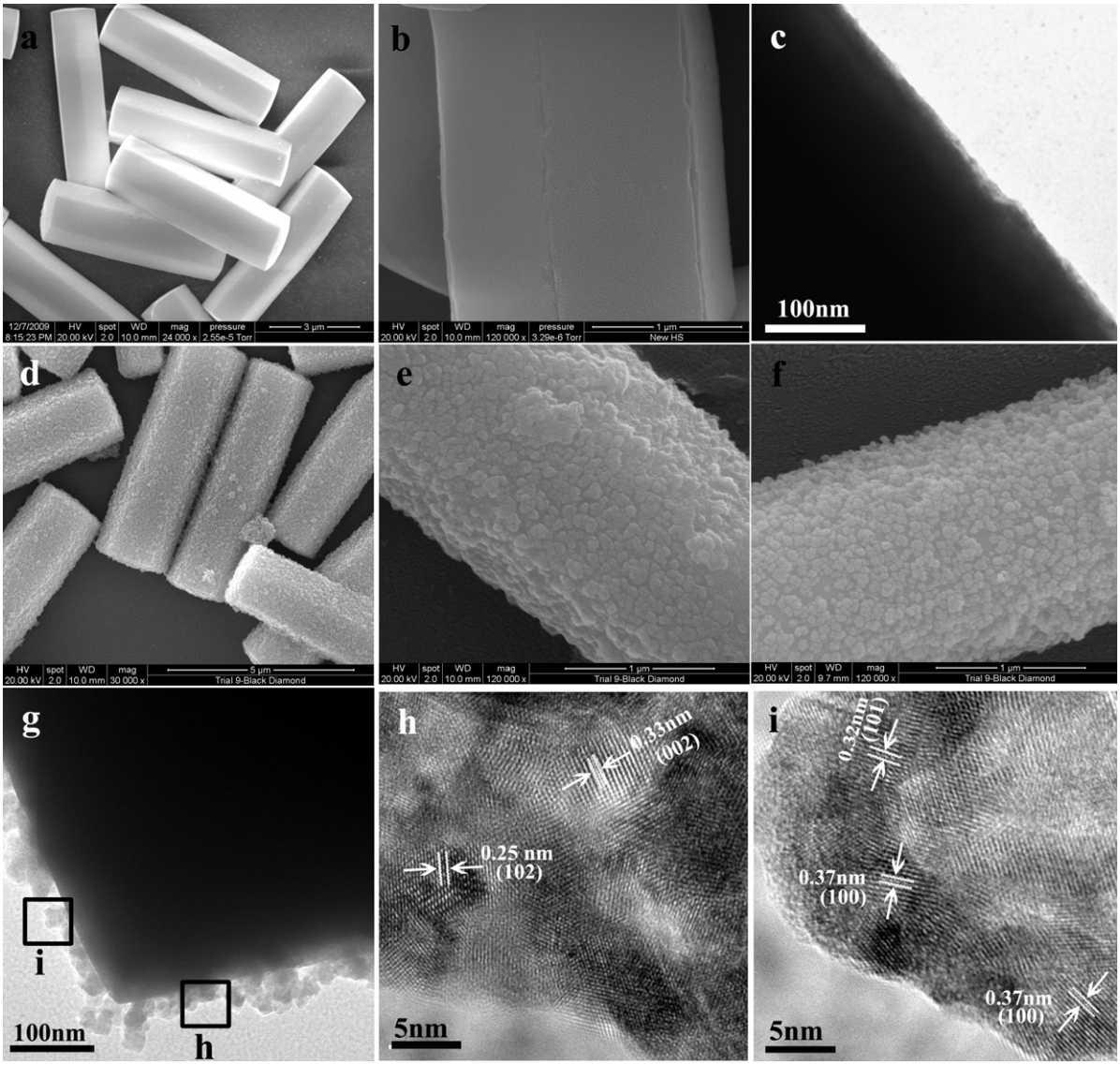

Fig. 1. SEM (a, b, d, e, and f) and TEM (c, g, h, and i) images of the products. (a–c) Pure $NaYF_4$:Yb,Tm and (d–i) $NaYF_4$:Yb,Tm/CdS composite. Figure h and i are the corresponding high-resolution TEM images from the areas outlined by the rectangles marked in (g).

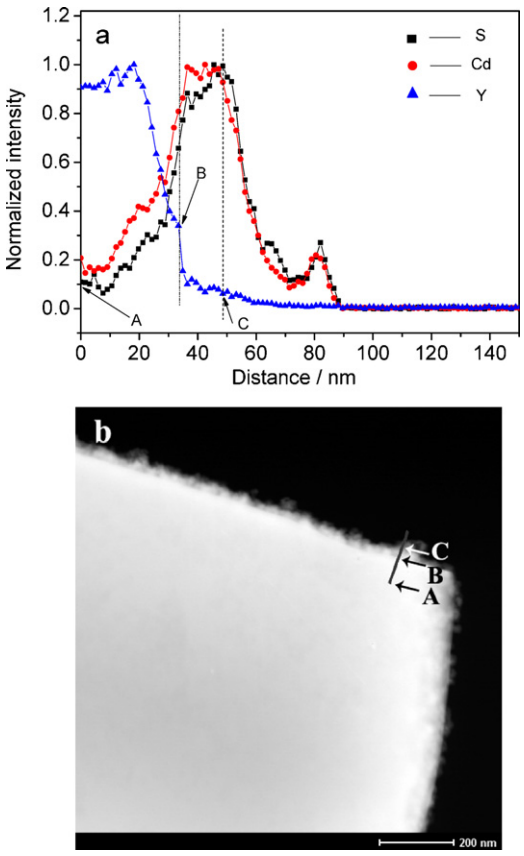

Fig. 2. EDX line scan profiles (a) and TEM (b) image of the $NaYF_4$:Yb,Tm/CdS composite. Points A–C in (a) are corresponding to the same points shown in (b). In figure (a), Y, Cd, and S data are plotted as blue triangles, red dots, and black rectangles, respectively. (For interpretation of the references to color in this figure legend, the reader is referred to the web version of the article.)

Scheme 1 shows the synthesis process for the NIR photocatalyst. CdS, a well-known low band gap semiconductor (about 2.5 eV) [33,34], is coupled to the hexagonal phase (β-phase) of $NaYF_4$:Yb,Tm microcrystals. The large microcrystals are known to have much higher upconversion efficiency than its nano-counterparters [35]. CdS nanoparticles are pretreated with thioglycolic acid molecules ($SHCH_2COOH$). The SH groups are for self-stabilization, and the COOH groups functionalize the surface. The surfaces of (β-phase) $NaYF_4$:Yb,Tm microcrystals are activated by the treatment with mercaptoethanol molecules ($SHCH_2CH_2OH$). The strong interaction between the –SH groups and lanthanide ions would leave many OH groups on the surface of the microcrystals. The subsequent reaction between mercaptoethanol and thioglycolic acid forms a stable $NaYF_4$:Yb,Tm/CdS composite.

2. Experimental

2.1. Chemicals

All the chemicals were used as received without further purification.

2.2. Synthesis of mercaptoethanol functionalized upconversion microrods

Pure $NaYF_4$:Yb,Tm microrods were synthesized via an ethylenediamine tetraacetic acid disodium salt (EDTA) assisted-hydrothermal method [36]. The molar ratio of lanthanide ions in the product, Y/Yb/Tm, is 79.5:20:0.5. Then 400 mg of the prepared

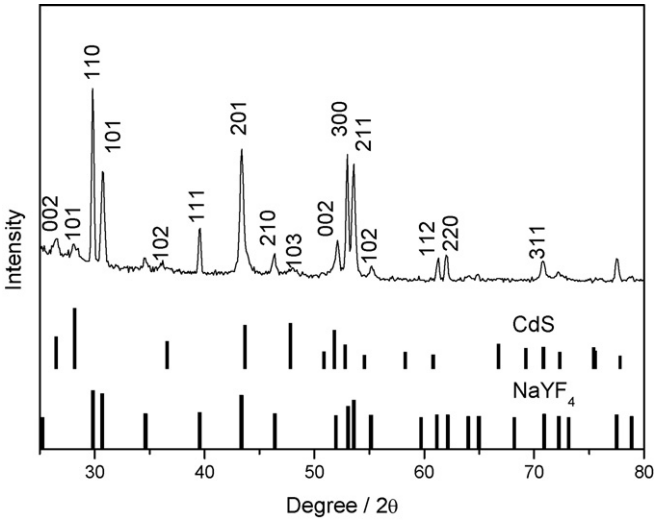

Fig. 3. XRD pattern of the prepared $NaYF_4$:Yb,Tm/CdS composite.

$NaYF_4$:Yb,Tm microcrystals were dispersed in 20 mL deionized water containing 0.2 mL mercaptoethanol. After stirring for 3 h, the product was separated and washed.

2.3. Synthesis of thioglycolic acid functionalized CdS nanoparticles

Pure CdS nanoparticles are prepared by a hydrothermal reaction [37]. Then 70 mg of CdS nanoparticles were treated with 10 mL deionized water containing 0.1 mL hioglycolic acid, stired for 3 h, then centrifuged and washed.

2.4. Preparation of $NaYF_4$:Yb,Tm/CdS composite

The $NaYF_4$:Yb,Tm and CdS precursors were mixed in 20 mL deionized water, then heated to 160 °C for 3 h. Then the yellow precipitates of $NaYF_4$:Yb,Tm/CdS were collected from the suspension by centrifugation (2000 rpm, 5 min) and washed with deionized water for several times. For comparison pure $NaYF_4$:Yb,Tm and CdS precursors which were not modified were mixed together, then treated the same conditions as described above.

2.5. Detection of photogenerated OH radicals

Terephthalic acid (4×10^{-4} M) was dissolved in NaOH (2×10^{-3} M) solution. In a typical process, 20 mg $NaYF_4$:Yb,Tm/CdS mixed with 10 mL of terephthalic acid solution. Then the mixture was irradiated with a NIR laser (λ = 976 nm). At every 30 min, 1.2 mL of the suspensions were collected, then centrifuged. Then 1 mL of the solution was diluted four times for the PL measurement. The hydroxyterephthalate anion formed was monitored by fluorescence analysis with a excitation wavelength of 320 nm. In the control experiments, pure CdS and $NaYF_4$:Yb,Tm were analyzed under identical conditions.

2.6. Photocatalytic activity measurements

The photocatalytic activities of the $NaYF_4$:Yb,Tm/CdS were measured by the degradation of Rhodamine B in an aqueous solution. 20 mg of photocatalyst was suspended in a 10 mL aqueous solution of Rhodamine B (10 ppm). Prior to irradiation, the suspension was stirred in the dark for 24 h to establish an adsorption/desorption equilibrium between the photocatalyst and Rhodamine B. Then the mixture was first irradiated with a NIR laser (λ = 976 nm,

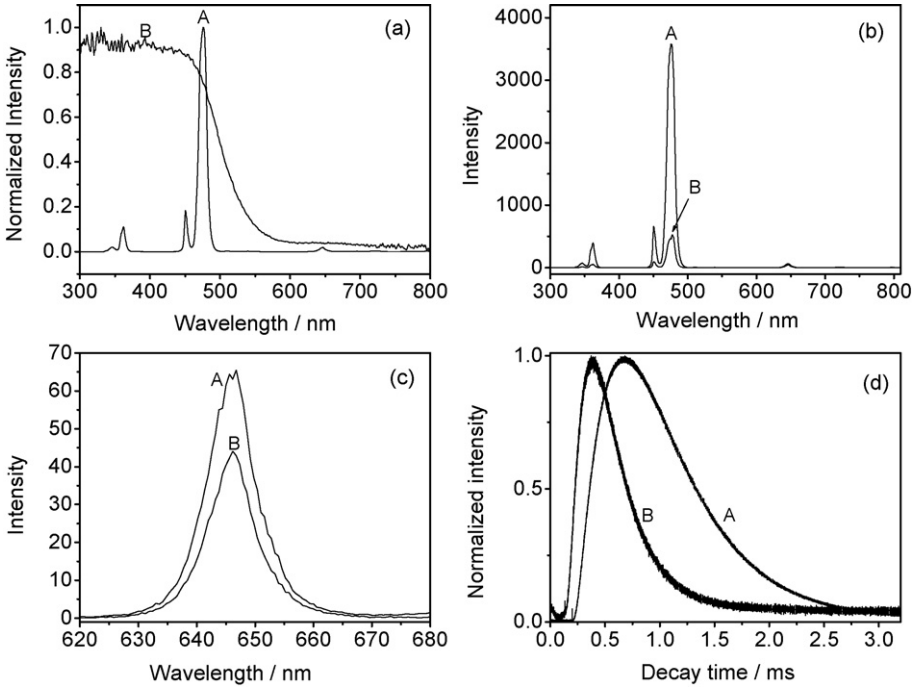

Fig. 4. (a): (A) Upconversion emission spectrum of $NaYF_4$:Yb,Tm and (B) absorption spectrum of CdS. (b and c) Upconversion emission spectra of (A) $NaYF_4$:Yb,Tm and (B) $NaYF_4$:Yb,Tm/CdS. (c) is the magnified spectrum of (b). (d) Time-resolved fluorescence decay curves of Tm^{3+} (λ_{em} = 476 nm) of (A) $NaYF_4$:Yb,Tm and (B) $NaYF_4$:Yb,Tm/CdS. All the upconversion emission spectra were recorded upon 976 nm NIR excitation.

power = 2W, beam diameter = 1 cm) for different hours. At 30 min intervals, 0.6 mL of the suspensions were collected, then centrifuged. Then 0.5 mL of the solution was diluted eight times for the following measurement. The concentration of Rhodamine B was measured by a UV–visible spectrophotometer and the absorption peak at 550 nm was monitored. The photocatalytic activity has also been demonstrated by using methylene blue as degradation probe. And the conditions are same as the degradation of Rhodamine B. Visible-light photocatalytic activity was done by dispersing 40 mg photocatalyst into 20 mL of aqueous solution containing 50 ppm Rhodamine B. The light source is a commercial 300 W tungsten halogen spotlight surrounded with a filter that restricted the illumination to the 400–660 nm range.

2.7. Characterization

The general morphology of the products was characterized by a field-emission scanning electron microscope (FESEM, FEI, Quanta

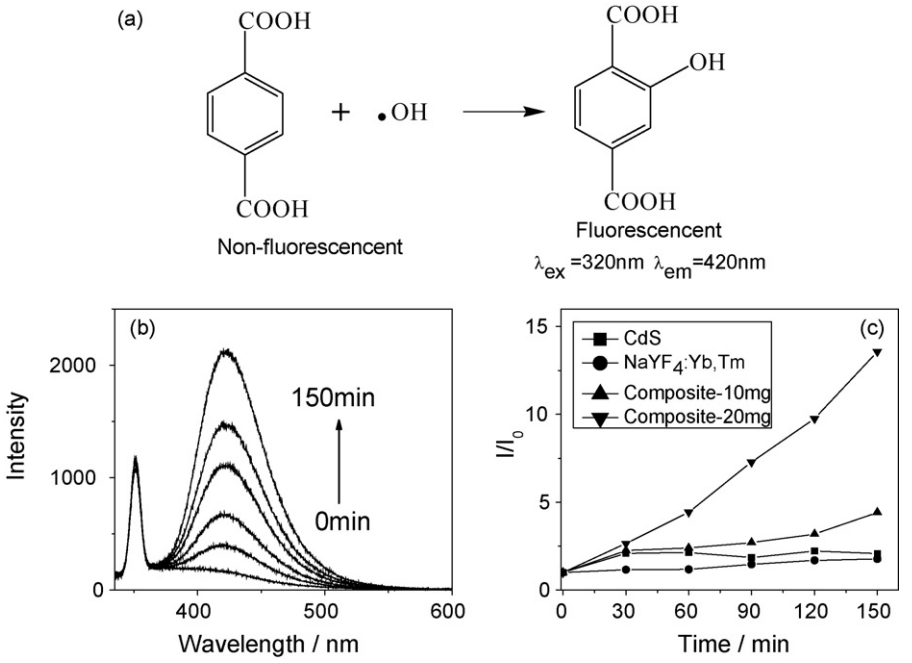

Fig. 5. (a) Reaction between the formed OH radicals and probe molecules, terephthalic acid. (b) Time-dependent fluorescence spectra of the terephthalic acid solution (4×10^{-4} M) containing 20 mg of $NaYF_4$:Yb,Tm/CdS composite upon NIR irradiation. (c) Fluorescence intensity of the emission peak at 420 nm as a function of NIR irradiation time.

400 FEG) equipped with an energy-dispersive spectroscopy instrument. TEM, HRTEM and EDX line scan profiles were carried out on a Tecnai F20 microscope (FEI, 200 kV) coupled with an energy-dispersive X-ray (EDX) spectrometer. X-ray diffraction (XRD) patterns were recorded using a Bruker D8 Advance diffractometer with high-intensity Cu $K\alpha_1$ irradiation ($\lambda = 1.5406$ Å). Room temperature upconversion fluorescence spectra were recorded on a Hitachi F-4500 fluorescence spectrophotometer equipped with a commercial 976 nm IR laser with tunable power. In lifetime measurements, a 980 nm laser line from Optical Parametric Oscillator (OPO) (Opotek MagicPRISM) was used for excitation, which was pumped by the third harmonics, 355 nm line of a Nd:YAG laser (Quantel Brilliant B). The pulse-width of laser was 4 ns and the photo-detector was using a thermoelectrically cooled GaAs photomultiplier tube (PMT) (Hamamatsu R636-10) with 3 ns response time. A 600 MHz oscilloscope (Agilent Infiniium 54830B) was used to record the decay-time spectrum by using an average of 512 times. A 10× amplifier was used to record the signal from the $NaYF_4$:Yb,Tm/CdS composite. UV–vis spectra were recorded on a Varian Cary 500 Scan UV–visible system.

3. Results and discussion

3.1. Morphology investigations

The size and morphology of the resulting materials were examined by SEM and TEM. Fig. 1a displays a representative SEM image of the pure $NaYF_4$:Yb,Tm microcrystals. The microrod crystals are of a length roughly equal to 6 μm and diameter of 1 μm. As shown in the magnified SEM image (Fig. 1b) and the TEM image (Fig. 1c), the surfaces of the microrods are rather smooth. However, the surfaces become rougher after the deposition of CdS (Fig. 1d). Fig. 1e and f presents the enlarged views of the single microrods. Clearly, CdS nanoparticles of 50–80 nm are uniformly assembled on the surface of the $NaYF_4$:Yb,Tm microrods. More detailed SEM images confirm the assembly (Fig. S2). In the TEM images (Figs. 1g and S3), the apparent microscopy contrast further confirms the presence of CdS nanoparticles on the surface of $NaYF_4$:Yb,Tm microrods. High-resolution TEM images (Fig. 1h and i) provide further insight into the microstructure of the coated nanoparticles. The clear lattice fringes indicate high crystallinity and the measured lattice spacings match very well with the planes of hexagonal phase CdS (JCPDS no. 75-1545). As seen from Fig. S4, the color of pure $NaYF_4$:Yb,Tm is white, while the composite becomes yellow. To find out if CdS could be coupled to $NaYF_4$ by physical adsorption, control experiments were carried out in the absence of chemical modifiers. As shown in Fig. S5, CdS does not adsorb well onto $NaYF_4$ without surface functionalization. The strong coupling between CdS and $NaYF_4$ is probably due to the formation of chemical bonds between thioglycolic acid and mercaptoethanol.

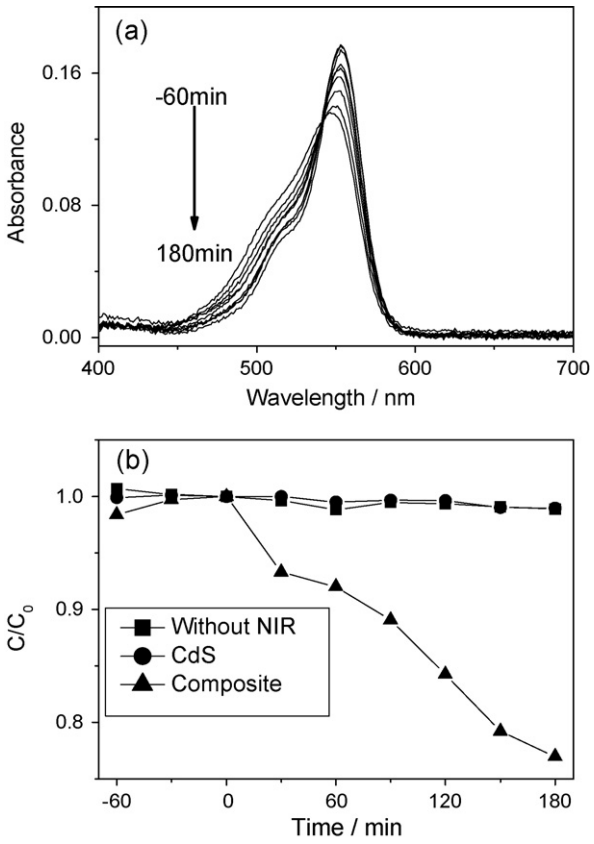

Fig. 6. (a) Time-dependent absorption spectra of Rhodamine B (10 ppm) solution containing $NaYF_4$:Yb,Tm/CdS composite upon NIR irradiation. (b) Rhodamine B reduction in UV–vis absorption spectra at 550 nm as a function of NIR irradiation time for different samples.

3.2. Composition studies

EDX elemental line scanning was performed to further determine the composition of composite, especially the particles on the surface. Fig. 2a shows the line scan profiles, recorded along the black line presented in Fig. 2b. The scanning starts from point A, where both the signal from $NaYF_4$:Yb,Tm and CdS are detected. The atomic ratio of Y/Cd is 17:0.4. It can be clearly seen from Fig. 2a that with the scanning going outside, the signal of Y drops, while Cd and S increase. At the interface (point B), Y/Cd decreases to 22:10. Fol-

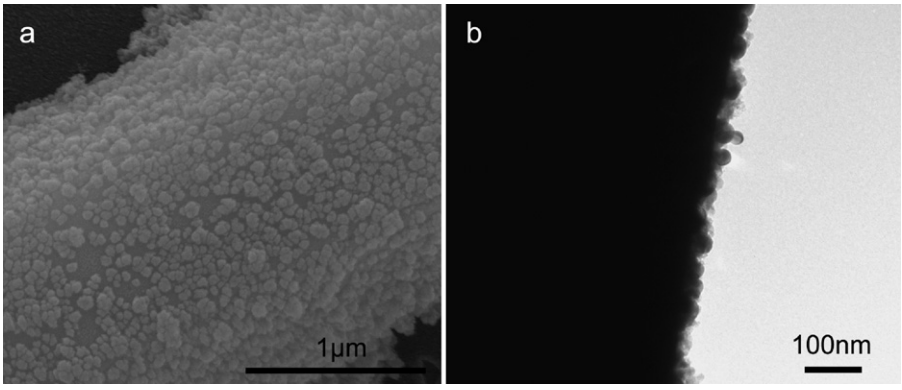

Fig. 7. SEM (a) and TEM (b) images of the $NaYF_4$:Yb,Tm/CdS composite after NIR photocatalysis (3 h).

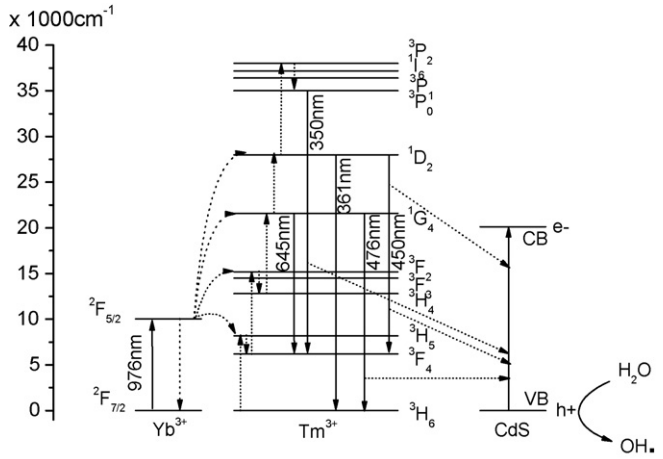

Fig. 8. Schematic illustration of energy transfer mechanism from $NaYF_4$:Yb,Tm to CdS upon 976 nm NIR irradiation.

lowing point B is a sharp decrease for Y. But Cd and S gradually grow to the maximum value at point C, where Y/Cd is 2:28. This a clear evidence for the strong coupling of CdS nanoparticles on the $NaYF_4$:Yb,Tm microcrystals.

A typical XRD pattern provides further crystallinity and phase information for the composite. As shown in Fig. 3, in addition to the reflections of hexagonal phase $NaYF_4$ (JCPDS no. 28-1192), several weak peaks of hexagonal phase CdS (JCPDS no. 75-1545) are observed at 26.5°, 28.1°, 36.4° and 48.1°.

3.3. Optical properties

NIR photocatalysis depends on the energy transfer from $NaYF_4$:Yb,Tm to CdS. The requirement for an efficient energy transfer is to make the donor emission band overlap with the absorption band of acceptor [38,39]. Here $NaYF_4$:Yb,Tm is the donor and CdS is the acceptor. The upconversion fluorescence spectrum of $NaYF_4$:Yb,Tm and the absorption spectrum of CdS are presented in Fig. 4a. $NaYF_4$:Yb,Tm could absorb NIR photons because the Yb^{3+} ion has a large absorption cross section from 970 to 1000 nm [40,41]. After absorbing two or more NIR photons, $NaYF_4$:Yb,Tm emits visible and UV light. As shown in Fig. 4a-A, five emission peaks appear upon NIR irradiation. The predominate blue emission peaks at 450 and 476 nm are assigned to the $^1D_2 \rightarrow {}^3F_4$, $^1G_4 \rightarrow {}^3H_6$ transitions of Tm^{3+} [42–46]. The two UV emissions at 350 and 361 nm are due to the $^3P_0 \rightarrow {}^3F_4$ and $^1D_2 \rightarrow {}^3H_6$ transitions, respectively [42–46]. The weakest red emission at 645 nm is from the $^1G_4 \rightarrow {}^3F_4$ transition [42–46]. As a semiconductor with low energy gap, CdS exhibits a broad absorption band from 200 to 550 nm. It is very clear that the absorption band of CdS overlaps very well with the blue emission peak of upconversion particles. The large spectral overlap indicates that the upconversion blue emission can be strongly quenched by energy transfer.

To examine the energy transfer process, the upconversion emission spectra of the upconversion/CdS composite were recorded upon 976 nm NIR excitation (Fig. 4b). The intensity of UV and blue emission peaks are greatly reduced after the combination of CdS, indicating significant energy transfer. However, it can be clearly observed from Fig. 4c that due to the small overlap with the absorption spectrum of CdS, the red emission peak of $NaYF_4$:Yb,Tm only decreases slightly. The fluorescence intensity ratio of I_{blue}/I_{red} for the composite is 11.9, which is much smaller than the value of 41.3 for the pure $NaYF_4$:Yb,Tm. Since the two spectra were recorded under identical conditions and the Tm content was the same, the decrease in I_{blue}/I_{red} strongly suggests an energy transfer from $NaYF_4$:Yb,Tm to CdS.

A comparison between the lifetimes of the donor alone and the donor–acceptor pairs could provide direct evidence on the energy transfer. The life time of the emission at 476 nm for $NaYF_4$:Yb,Tm and $NaYF_4$:Yb,Tm/CdS were recorded (Fig. 4d). As the addition of CdS quenched the 476 nm emission, a 10× amplifier was used when measuring the $NaYF_4$:Yb,Tm/CdS sample. This caused a shorter rising time (about 0.4 ms, Curve B) than the pure $NaYF_4$:Yb,Tm (about 0.7 ms, Curve A). It should be noted that the signal amplification only affects the rise up time but has no effect on the decay-time measurements. The decay profiles are fit with monoexponential model. The average decay times are 788, and 359 μs for the pure $NaYF_4$:Yb,Tm and $NaYF_4$:Yb,Tm/CdS, respectively. The decrease in lifetime further confirms the energy transfer. The efficiency of energy transfer can be calculated from the following equation [47]:

$$E = 1 - \frac{\tau_{DA}}{\tau_D}$$

where τ_{DA} and τ_D are the lifetime of $NaYF_4$:Yb,Tm with and without CdS, respectively. The observed energy transfer efficiency of the blue emissions is 54.4%.

Photocatalysis generates hydroxyl radicals which are responsible for the degradation of pollutant molecules. Herein we applied a universally used method, photoluminescence technique [48–50], to monitor the formation of hydroxyl radicals upon NIR irradiation on the $NaYF_4$:Yb,Tm/CdS composite. Terephthalic acid is a traditional fluorescent probe [48–50]. As shown in Fig. 5a, the non-fluorescent terephthalic acid captures hydroxyl radicals to produce the highly fluorescent 2-hydroxyterephthalic acid with an emission peak at 420 nm upon excitation wavelength of 320 nm. Therefore, hydroxyl radicals can be monitored by the fluorescence intensity changes. The measurement results are shown in Fig. 5b. The fluorescence intensity increases nearly linearly with irradiation time, which is similar to the previous observation [48–50]. This is a clear indication of OH radicals formation. For comparison, we carried out the control experiments involving pure CdS or $NaYF_4$:Yb,Tm. No capability of producing OH radicals is observed from Fig. 5c. And the amount of generated OH radicals is also dependent on the concentration of photocatalyst. The detailed spectra are shown in Fig. S6.

3.4. Photocatalytic properties

The NIR-driven photocatalytic activity of the $NaYF_4$:Yb,Tm/CdS composite was measured by the degradation of Rhodamine B in an aqueous solution. Prior to the photoirradiation, all the samples were suspended in the Rhodamine B aqueous solution for one day to establish the adsorption/desorption equilibrium of dye on the sample surface, then pretreated with NIR for 1 h. It can be seen from Fig. 6a that the absorbance of Rhodamine B gradually decreases with the NIR irradiation, suggesting the occurrence of photocatalysis. In the control experiments, no photocatalytic activity could be observed as shown in Figs. 6b and S7. To further demonstrate the photoactivity, NIR driven photocatalytic degradation of methylene blue has also been performed as shown in Fig. S8. Since CdS is a good visible-light photocatalyst, the composite also show high photoactivity under visible-light (Fig. S9).

It has been reported that under strong UV or visible-light irradiation CdS could be oxidized by photogenerated holes to release Cd^{2+} ions [51]. The photostability of the $NaYF_4$:Yb,Tm/CdS composite was investigated. The CdS nanoparticles were intact after exposing to NIR for 3 h (Fig. 7). The concentration of Cd^{2+} ions in the solution was also measured by ICP-AES before and after photocatalysis. As shown in Table S1, there is no evident increase of Cd^{2+} ions after

photocatalysis. The good photostability is not surprising because of the very mild visible-light intensity in this NIR-induced system. Moreover, the modification with thioglycolic acid could provide a protective effect [49,52,53].

3.5. Mechanisms

The mechanism for the NIR-driven photocatalysis is shown in Fig. 8. The absorption of pump photons populates the $^2F_{5/2}$ level in Yb^{3+}. A Tm^{3+} ion is excited to the $^3H_5$ level by the energy transferred from the excited Yb^{3+}, and then relaxes nonradiatively to the $^3F_4$ level. Energy transfer from another Yb^{3+} ion to the Tm^{3+} causes the formation of a $^3F_2$ level. Subsequently, the Tm^{3+} relaxes to the $^3H_4$ level and then is excited to the $^1G_4$ level by absorbing energy from another excited Yb^{3+}. The sequential energy absorption from two excited Yb^{3+} ions promotes Tm^{3+} to $^1D_2$ and $^3P_2$. Then the excited Tm^{3+} ions fall to lower energy levels. $^1D_2 \rightarrow {}^3F_4$, $^1G_4 \rightarrow {}^3H_6$, $^3P_0 \rightarrow {}^3F_4$, $^1D_2 \rightarrow {}^3H_6$ and $^1G_4 \rightarrow {}^3F_4$ transitions produce the blue emissions at 450 nm, 470 nm, UV emissions at 350 nm, 361 nm and red emission at 645 nm, respectively [42–46]. Here the $^1G_4$ level is the predominant excited state in this material as suggested by the strongest blue emission. For CdS [54], the energy gap from valence band (VB) to conduction band (CB) is about 2.5 eV which is lower than the emitted blue and UV photon energy. As well known, semiconductors could be excited by the photons with an energy equivalent to or higher than the band gap energy, which causes the formation of photoelectrons and holes. According to the SEM images, $NaYF_4$:Yb,Tm and CdS are very close to each other. These allow energy transfer from $NaYF_4$:Yb,Tm to CdS. Then the excited CdS triggers photocatalysis.

4. Conclusions

In summary, we have explored a simple, efficient method to synthesize a novel NIR photocatalyst, the $NaYF_4$:Yb,Tm/CdS composite. The morphology and composition of the resulting photocatalyst were investigated. The energy transfer from $NaYF_4$:Yb,Tm to CdS upon NIR irradiation was confirmed. The NIR-driven photocatalysis was realized by degrading Rhodamine B and methylene blue. This study suggests a promising system to study NIR photocatalysis, which may have profound implication on the future utilization of solar energy.

Acknowledgements

This work was supported by a Strategic Investments Scheme administrated by The Chinese University of Hong Kong. We thank Prof. K.W. Cheah and Dr. K.F. Li (Department of Physics, Hong Kong Baptist University) for the lifetime measurements.

Appendix A. Supplementary data

Supplementary data associated with this article can be found, in the online version, at doi:10.1016/j.apcatb.2010.08.017.

References

[1] M.A. Fox, M.T. Dulay, Chem. Rev. 93 (1993) 341–357.
[2] A. Fujishima, K. Honda, Nature 238 (1972) 37–38.
[3] M.R. Hoffmann, S.T. Martin, W.Y. Choi, D.W. Bahnemann, Chem. Rev. 95 (1995) 69–96.
[4] Y. Chen, D.D. Dionysiou, Appl. Catal. B: Environ. 69 (2006) 24–33.
[5] C. Guillard, B. Beaugiraud, C. Dutriez, J.-M. Herrmann, H. Jaffrezic, N. Jaffrezic-Renault, M. Lacroix, Appl. Catal. B: Environ. 39 (2002) 331–342.
[6] H. Lin, C.P. Huang, W. Li, C. Ni, S.I. Shah, Y.-H. Tseng, Appl. Catal. B: Environ. 68 (2006) 1–11.
[7] S. Yamazoe, Y. Hitomi, T. Shishido, T. Tanaka, Appl. Catal. B: Environ. 82 (2008) 67–76.
[8] X. Chen, S.S. Mao, Chem. Rev. 107 (2007) 2891–2959.
[9] Y. Ishibai, J. Sato, T. Nishikawa, S. Miyagishi, Appl. Catal. B: Environ. 79 (2008) 117–121.
[10] X. Yang, C. Cao, L. Erickson, K. Hohn, R. Maghirang, K. Klabunde, Appl. Catal. B: Environ. 91 (2009) 657–662.
[11] V. Iliev, D. Tomova, L. Bilyarska, A. Eliyas, L. Petrov, Appl. Catal. B: Environ. 63 (2006) 266–271.
[12] T.W. Kim, S.G. Hur, S.J. Hwang, H. Park, W. Choi, J.H. Choy, Adv. Funct. Mater. 17 (2007) 307–314.
[13] Y. Park, W. Kim, H. Park, T. Tachikawa, T. Majima, W. Choi, Appl. Catal. B: Environ. 91 (2009) 355–361.
[14] S. Higashimoto, M. Azuma, Appl. Catal. B: Environ. 89 (2009) 557–562.
[15] J.C. Kim, J. Choi, Y.B. Lee, J.H. Hong, J.I. Lee, J.W. Yang, W.I. Lee, N.H. Hur, Chem. Commun. (2006) 5024–5026.
[16] J.C. Yu, W.K. Ho, J.G. Yu, H. Yip, P.K. Wong, J.C. Zhao, Environ. Sci. Technol. 39 (2005) 1175–1179.
[17] Y.Y. Huang, F.Q. Sun, H.J. Wang, Y. He, L.S. Li, Z.X. Huang, Q.S. Wu, J.C. Yu, J. Mater. Chem. 19 (2009) 6901–6906.
[18] C. Radhakrishnan, M.K.F. Lo, M.V. Warrier, M.A. Garcia-Garibay, H.G. Monbouquette, Langmuir 22 (2006) 5018–5024.
[19] K. Sayama, H. Hayashi, T. Arai, M. Yanagida, T. Gunji, H. Sugihara, Appl. Catal. B: Environ. 94 (2010) 150–157.
[20] W. Morales, M. Cason, O. Aina, N.R. de Tacconi, K. Rajeshwar, J. Am. Chem. Soc. 130 (2008) 6318–6319.
[21] G.S. Li, D.Q. Zhang, J.C. Yu, Chem. Mater. 20 (2008) 3983–3992.
[22] X. Zhao, T. Xu, W. Yao, C. Zhang, Y. Zhu, Appl. Catal. B: Environ. 72 (2007) 92–97.
[23] X.C. Wang, K. Maeda, A. Thomas, K. Takanabe, G. Xin, J.M. Carlsson, K. Domen, M. Antonietti, Nat. Mater. 8 (2009) 76–80.
[24] J. Bai, J. Li, Y. Liu, B. Zhou, W. Cai, Appl. Catal. B: Environ. 95 (2010) 408–413.
[25] G.S. Li, D.Q. Zhang, J.C. Yu, Environ. Sci. Technol. 43 (2009) 7079–7085.
[26] W.P. Qin, D.S. Zhang, D. Zhao, L.L. Wang, K.Z. Zheng, Chem. Commun. (2010) 2304–2306.
[27] S. Heer, K. Kompe, H.U. Gudel, M. Haase, Adv. Mater. 16 (2004) 2102–2105.
[28] Y. Il Park, J.H. Kim, K.T. Lee, K.S. Jeon, H. Bin Na, J.H. Yu, H.M. Kim, N. Lee, S.H. Choi, S.I. Baik, H. Kim, S.P. Park, B.J. Park, Y.W. Kim, S.H. Lee, S.Y. Yoon, I.C. Song, W.K. Moon, Y.D. Suh, T. Hyeon, Adv. Mater. 21 (2009) 4467–4471.
[29] S.J. Budijono, J.N. Shan, N. Yao, Y. Miura, T. Hoye, R.H. Austin, Y.G. Ju, R.K. Prud'homme, Chem. Mater. 22 (2010) 311–318.
[30] K.W. Kramer, D. Biner, G. Frei, H.U. Gudel, M.P. Hehlen, S.R. Luthi, Chem. Mater. 16 (2004) 1244–1251.
[31] Y. Wei, F.Q. Lu, X.R. Zhang, D.P. Chen, Chem. Mater. 18 (2006) 5733–5737.
[32] F. Auzel, Chem. Rev. 104 (2004) 139–173.
[33] T.Y. Zhai, X.S. Fang, Y. Bando, B. Dierre, B.D. Liu, H.B. Zeng, X.J. Xu, Y. Huang, X.L. Yuan, T. Sekiguchi, D. Golberg, Adv. Funct. Mater. 19 (2009) 2423–2430.
[34] Y.F. Lin, J. Song, Y. Ding, S.Y. Lu, Z.L. Wang, Adv. Mater. 20 (2008) 3127–3130.
[35] J.N. Shan, Y.G. Ju, Nanotechnology 20 (2009) 275603.
[36] Y.J. Sun, Y. Chen, L.J. Tian, Y. Yu, X.G. Kong, J.W. Zhao, H. Zhang, Nanotechnology 18 (2007) 275609.
[37] G.F. Lin, J.W. Zheng, R. Xu, J. Phys. Chem. C 112 (2008) 7363–7370.
[38] N. Kameta, M. Masuda, H. Minamikawa, Y. Mishima, I. Yamashita, T. Shimizu, Chem. Mater. 19 (2007) 3553–3560.
[39] M.A. Oar, J.A. Serin, W.R. Dichtel, J.M.J. Frechet, Chem. Mater. 17 (2005) 2267–2275.
[40] G. Boulon, A. Collombet, A. Brenier, M.T. Cohen-Adad, A. Yoshikawa, K. Lebbou, J.H. Lee, T. Fukuda, Adv. Funct. Mater. 11 (2001) 263–270.
[41] R. Martin-Rodriguez, R. Valiente, S. Polizzi, M. Bettinelli, A. Speghini, F. Piccinelli, J. Phys. Chem. C 113 (2009) 12195–12200.
[42] G.S. Yi, G.M. Chow, Adv. Funct. Mater. 16 (2006) 2324–2329.
[43] L.Y. Wang, Y.D. Li, Chem. Mater. 19 (2007) 727–734.
[44] F. Zhang, Y.F. Shi, X.H. Sun, D.Y. Zhao, G.D. Stucky, Chem. Mater. 21 (2009) 5237–5243.
[45] J. Yang, C.M. Zhang, C. Peng, C.X. Li, L.L. Wang, R.T. Chai, J. Lin, Chem. Eur. J. 15 (2009) 4649–4655.
[46] Z.Q. Li, Y. Zhang, Nanotechnology 19 (2008) 345606.
[47] H. Lu, O. Schops, U. Woggon, C.M. Niemeyer, J. Am. Chem. Soc. 130 (2008) 4815–4827.
[48] K. Ishibashi, A. Fujishima, T. Watanabe, K. Hashimoto, Electrochem. Commun. 2 (2000) 207–210.
[49] V. Rajendran, M. Lehnig, C.M. Niemeyer, J. Mater. Chem. 19 (2009) 6348–6353.
[50] C. Bohne, K. Faulhaber, B. Giese, A. Hafner, A. Hofmann, H. Ihmels, A.K. Kohler, S. Pera, F. Schneider, M.A.L. Sheepwash, J. Am. Chem. Soc. 127 (2005) 76–85.
[51] D. Meissner, R. Memming, B. Kastening, J. Phys. Chem. 92 (1988) 3476–3483.
[52] T. Rajh, A.E. Ostafin, O.I. Micic, D.M. Tiede, M.C. Thurnauer, J. Phys. Chem. 100 (1996) 4538–4545.
[53] W. Bae, R.K. Mehra, J. Inorg. Biochem. 70 (1998) 125–135.
[54] R.B. Little, M.A. El-Sayed, G.W. Bryant, S. Burke, J. Chem. Phys. 114 (2001) 1813–1822.